Res. Rep. Fac. Eng. Mie Univ., Vol. 17, pp. 103-122 (1992)

Review

Synthesis of Copper Oxide Superconductors under High Oxygen Pressure

Yasuo TAKEDA, Nobuyuki IMANISHI and Osamu YAMAMOTO
(Department of Chemistry for materials)

(Recieved August 26, 1992)

Effects of high oxygen pressure have been studied on the formation, structure and physical properties of Cu-oxides with perovskite-related structure. Wide range of oxygen deficiencies were realized in $LaCuO_{3-z}$ by changing the synthetic oxygen pressures. The transition metal doped 123 type superconductors, $RBa_2Cu_{3-x}M_xO_z$ (R:Y, Gd; M:Fe, Co) prepared under high oxygen pressure are good example in which we can see the very clear microdomain formation. The YBCO related superconductor, $YBaSrCu_3O_z$, showed the structural change on XRD observation from orthorhombic to tetragonal when oxygen was over-doped above z=7.0. The "tetragonal phase" was also due to the microdomain formation and the XRD pattern was only averaged one. $La_{2-x}A_xCuO_{4+z}$ with A=Nd and Bi having various oxygen content was prepared under high oxygen pressure and the electrochemical oxidation. They showed large superconducting volume fractions by oxygen dope. The known microscopic phase separation into nearly stoichiometric La_2CuO_4 and superconducting La_2CuO_{4+z} seems to be suppressed by the chemical substitution in the rock salt layers.

Key wards: high-Tc superconductor, high oxygen pressure, microdomain, electrochemical oxidation, $LaCuO_{3-z}$, $YBa_2Cu_{3-x}Fe_xO_z$, $YBaSrCu_3O_{7+z}$, $La_{2-x}Bi_xCuO_{4+z}$, $La_{2-x}Nd_xCuO_4$

1. Introduction

Reactions in oxygen gas at high temperature and pressure make it possible to produce oxides with controlled lattice defects, or oxides of transition metals of high valences which exist stably only in oxidizing atmosphere. After the 1986 discovery of superconductivity in cooper oxide[1], doped La_2CuO_4, the oxygen state of copper in CuO_2 plane and oxygen nonstoichiometry in the structure have been known to give an important rule to the superconductivity. The known copper-oxide superconductors all crystallize with intergrowth structures consisting of superconductive oxide layers alternating with nonsuperconductive oxide layer (so called infinite structure, $ACuO_2$, is only exception[2]). The superconductive layers have a fixed oxygen content and contain CuO_2 plane(s). The nonsuperconductive oxide layers have a variable oxygen content. Oxidation/reduction of the CuO_2 layers above/below the formal oxidation state $(CuO_2)^{2-}$ is a necessary condition to induce superconductivity. The superconductors have a mixed valence in the CuO_2 layers.

Oxidation of the CuO_2 layers gives p-type superconductivity; reduction of the CuO_2 layers gives n-type superconductivity. The non-superconductive intergrowth layers strongly influence the oxidation state of CuO_2 layers. It is very interesting to see the change of the structure and properties of superconductors when the oxygen is doped in the intergrowth layers. In this review, we present the several examples, $LaCuO_{3-z}$, $RBa_2Cu_{3-x}M_xO_z$ (R:Y, Gd; M:Fe,Co,Ni,Zn), $YBaSrCu_3O_{7+z}$, $La_{2-x}A_xCuO_{4+z}$ ($A=Nd^{3+}$, Bi^{3+}), which have been studied in our group.

2. Apparatus

We briefly describe the methods for generating the high oxygen pressure. For the experiment up to several hundred bars of oxygen gas below 800°C, the autoclaves for the hydrothermal synthesis are used. Figure 1 shows the simple system used in our laboratory. The material of the autoclave is made of cobalt and nickel based Hastelloy alloy, Stellite No. 25[3]. The generation of higher oxygen pressure needs the some contrivance. Figure 2 illustrates the apparatus we used to prepare $CaFeO_3$[4]. The girdle-type high pressure apparatus was combined with a sandwich type cell charged with powders of the starting material and an oxygen generator, CrO_3 or $KClO_4$. To prevent the direct reaction of these materials, a ZrO_2 disk was interposed. After applying a pressure of 15-60kbar, the platinum cell was heated to 900-1100°C to promote release of oxygen from the peroxide and absorption by oxygen deficient starting material. In the present study, we also used the same type of apparatus.

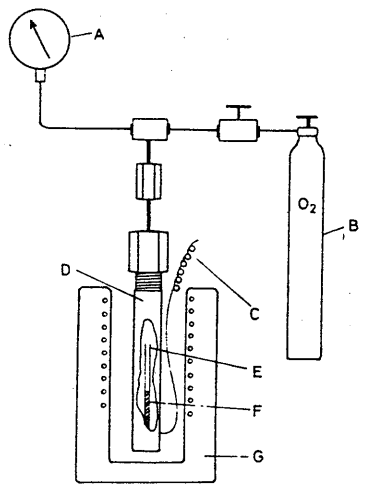

Fig.1 High oxygen pressure apparatus for 100bar. A: Bourdon gauge, B: oxygen resorvoir, C: thermocouple, D: reactor, E: gold tube, F: sample, and G: furnace

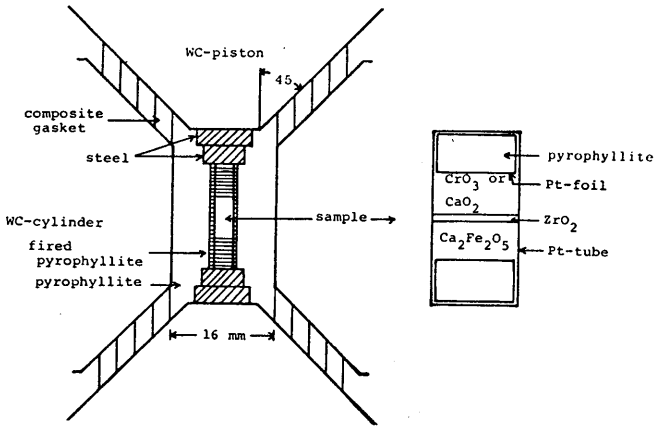

Fig.2 Sandwich type cell for very high oxygen pressure generation. In this figure girdle-type high pressure apparatus is shown. In the case of superconductors, peroxide $KClO_4$ was used.

3. $LaCuO_{3-z}$[5]

It had been believed for a long time that only mono- and di-valent states of copper are stable in oxides until Demazeau et al. synthesized $LaCuO_3$ having pure tri-valent oxidation state of copper under high oxygen pressure of 60kbar[6]. This compound had a perovskite structure formed by the three-dimensional $Cu^{3+}O_6$ network and showed metallic behavior and Pauli paramagnetism[7]. Another example having Cu^{3+} state was K_2NiF_4 type $La_2(Li_{0.5}Cu_{0.5})O_4$ prepared by same group, which was insulator due to the isolated arrangement of $Cu^{3+}O_6$ octahedra[6]. The both were the only known examples until the discovery of copper high T_c superconductor. $LaCuO_3$ is an important oxide in comparison with the copper superconductive oxides, because it has three dimensional CuO_6 network. Recently, the use the reactive starting materials made it possible to prepare $LaCuO_{3-z}$ (but not stoichiometric) under relatively mild conditions[8]. For example, $LaCuO_{3-z}$ can be prepared, as reported by Arjomand et al[9], from the each starting oxide, La_2O_3 and CuO at PO_2=400bar and 800°C, however the reaction temperature is too low to remove the impurity phase. We found the easy route to prepare the pure $LaCuO_{3-z}$ from $La_2Cu_2O_5$ which can be prepared at 1000°C for 10h in air. The phase, $La_2Cu_2O_5$, which is found by Cava et al.[10] is stable in very narrow temperature range such as between 999°C and 1025°C in air. This oxide is not perovskite related structure, and has an one-dimensional chain structure. The treatment of this phase under 100bar of oxygen pressure at 800°C brings the monoclinic perovskite $LaCuO_{2.75}$ and further annealing under higher pressure and at lower temperature dopes the oxygen to $LaCuO_{3-z}$(z>0.05). The reduction of the perovskite $LaCuO_{3-z}$ with Ti or Fe metals as an oxygen getter in a vacuum sealed Pyrex tube at 300-500°C makes more oxygen deficient $LaCuO_{2.5-2.6}$ (monoclinic) which has a different structure with $La_2Cu_2O_5$ used as the starting material

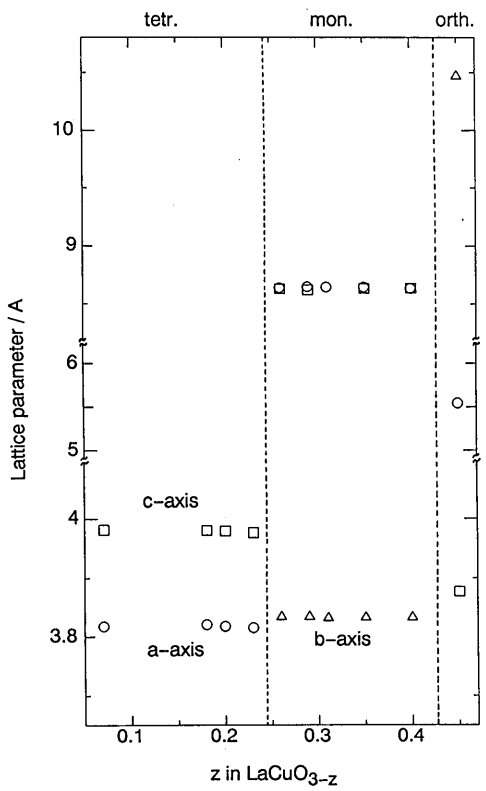

Fig.3 Variation of cell constants on oxygen content in the system, $LaCuO_{3-z}$.

although both have a similar composition. We can get a wide range of oxygen content such as $LaCuO_{2.50}$ - $LaCuO_{2.95}$ by these methods. The variation of lattice parameters on the oxygen content is shown in Fig.3. The oxygen stoichiometric $LaCuO_3$ (rhombohedral) could not be prepared by our method, which may need higher oxygen pressure. Figure 4 shows the electrical resistivity of samples having various oxygen contents. This system shows metallic conductivity even for a large amount of oxygen vacancy (z=0.25). The Seebeck coefficient measurement showed that the dominant carrier is hole in this system.

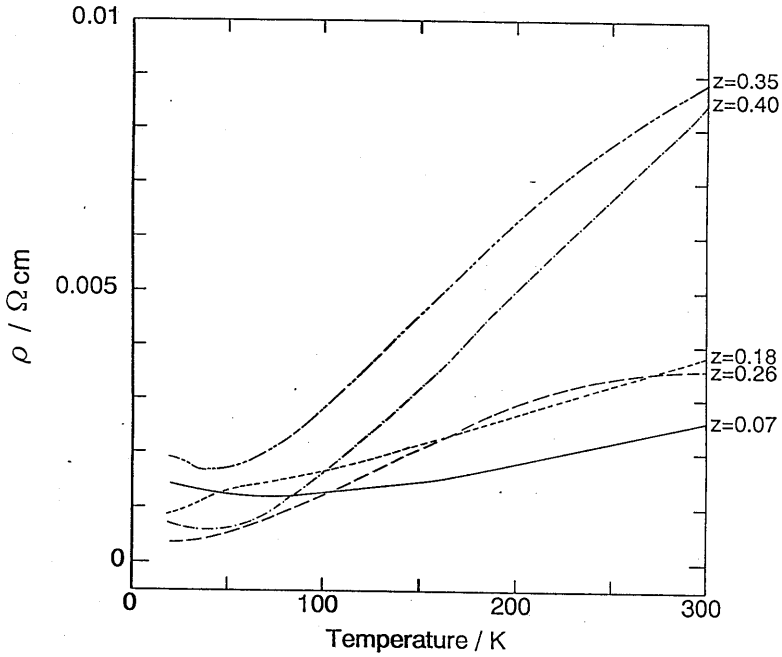

Fig.4. Temperature dependence of the resistivity in $LaCuO_{3-z}$.

4. $RBa_2Cu_{3-x}M_xO_y$ (R:Y, Gd; M:Fe,Co,Ni,Zn)[11]

The Fe- and Co-doped systems and the Ni- and Zn-doped systems have been found to behave differently. Both the Fe- and Co doped samples showed tetragonal XRD patterns for x>0.09, while the Ni- and Zn-doped samples remained orthorhombic throughout their single phase regions[12]. And oxygen content and T_c were considerably influenced by the high PO_2 treatment only in the former two systems[13,14]. Some relevant data are shown in Fig.5.

Figure 5(c) illustrates how the superconducting transition was influenced by the treatment at PO_2=100bar through the temperature dependence of the ac susceptibility ($\chi=\chi'+i\chi''$) of sintered $GdBa_2Cu_{2.88}Fe_{0.12}O_z$. Before the annealing, a diamagnetic response due to the Meissner effect ($-\chi$) could be seen below 62K, while the resistance of the same sample began to drop at 70K. The superconducting volume remained too small for 62K<T<70K to be detected by the magnetic measurement. It is easy to find in Fig.5(c) signs of an improved transition after the annealing; the magnetic and electrical measurements became consistent apparently. The χ'' peaks, found to arise from samples, became simple[15]. The annealing must have brought about chemical and structural changes improving the transition within individual particles and, thereby, automatically smoothing the intergrain coupling.

Microscopic structure of "tetragonal" Fe- and Co-doped samples were carefully examined by TEM, because we felt a similarity between these systems and $SrFe_{1-x}V_xO_{2.5+x}$[16]. In the Sr-Fe-V-O system also,

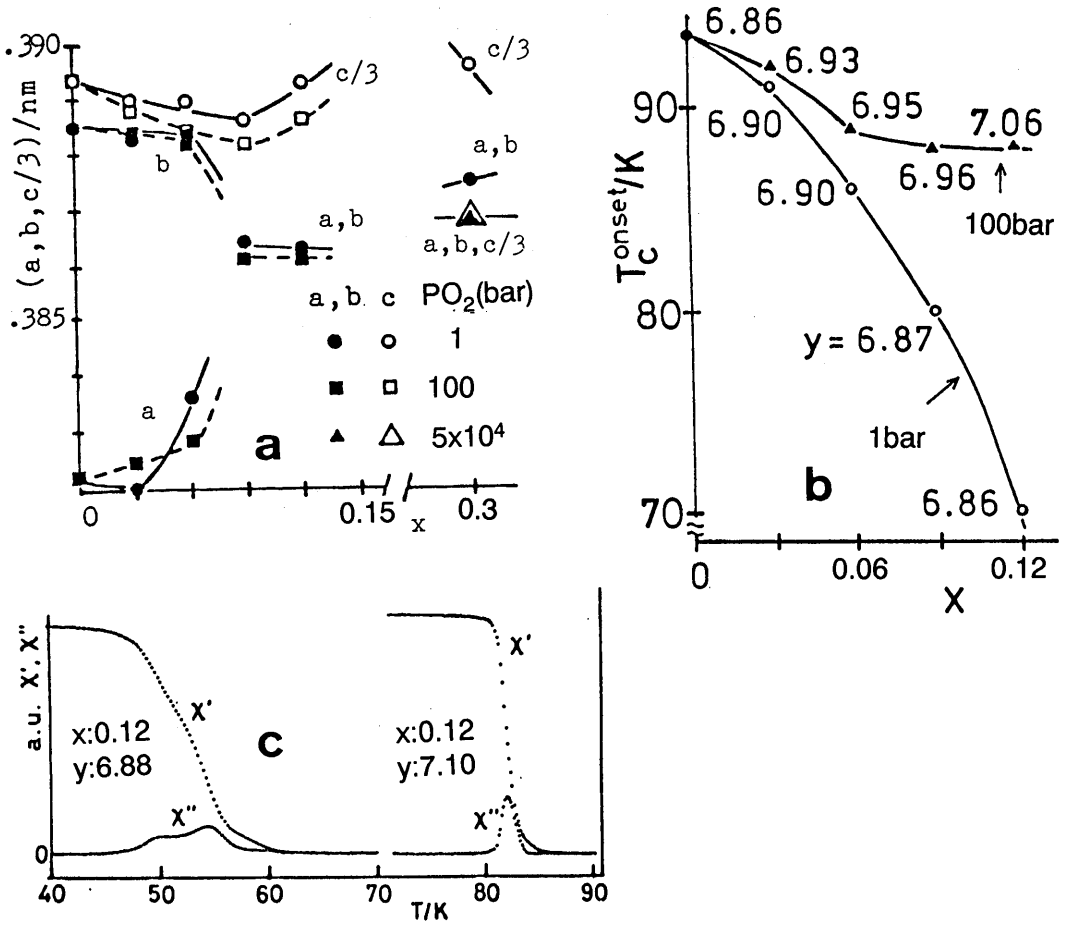

Fig.5 (a) Lattice constants of $YBa_2Cu_{3-x}Fe_xO_z$ (z being given in Fig.5b). (b) T_c of the same system as a function of x and z. (c) The ac susceptibility of $GdBa_2Cu_{2.88}Fe_{0.12}O_z$ before and after the annealing at PO_2=100bar.

a small amount of V impurity induced a transition to more symmetric structure as found by XRD, but TEM observation revealed that ordered domains were so small and so coherently packed that XRD gave only "averaged" high symmetry.

Electron micrographs of $YBa_2Cu_{3(1-x)}M_{3x}O_z$ (M:Fe, Co) varied from an ordinary (110) twinning pattern for x<0.06 to crossed fringes running along the [110] and [110] directions for x>0.09[17]. Both the twin band width and the fringe spacing tends to become narrower with increasing x. This tendency was little influenced by the treatment at PO_2=100bar, indicating that the change in microstructure was mostly controlled by the impurities. A typical high-resolution image and a corresponding diffraction pattern for (M,x,z)=(Fe, 0.12, 6.86) are shown in Fig.6. These have interpreted as arising from such a microdomain structure as shown in Fig.6(c)[16]. 1D Cu(1)-O chains are ordered in microdomains, while their direction changes by $\pi/2$ within the ab plane from domain to domain. The dark band in Fig.6(a) correspond to domain boundaries, and the diffraction spots are streaked along both the $[110]^*$ and $[110]^*$ directions in Fig.6(b) because of the small domain size (25-100nm^2). As discussed in [14,17], Fe and Co ions, if at least partially coordinated octahedrally, can trigger the microdomain structure formation.

We have found that heavily doped $YBa_2Cu_{2.7}Fe_{0.3}O_z$ even show superconducting behavior at so

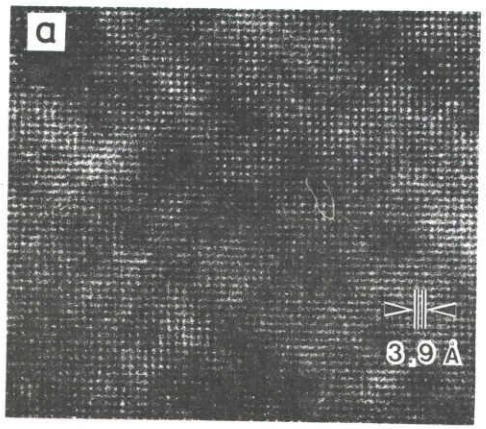

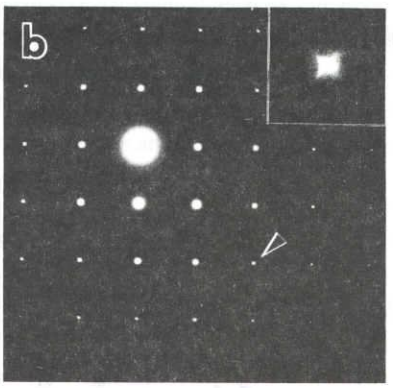

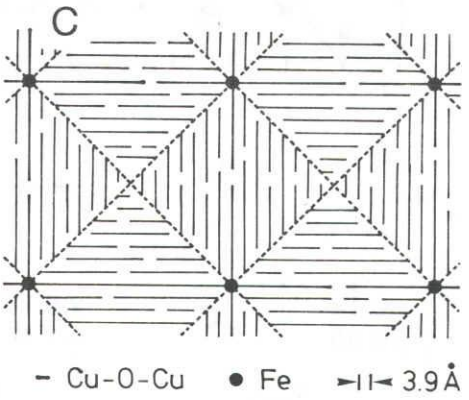

Fig.6 High-resolution micrograph(a) and the corresponding diffraction pattern(b) of $YBa_2Cu_{2.88}Fe_{0.12}O_{6.86}$, and microdomain structure (see text) (c).

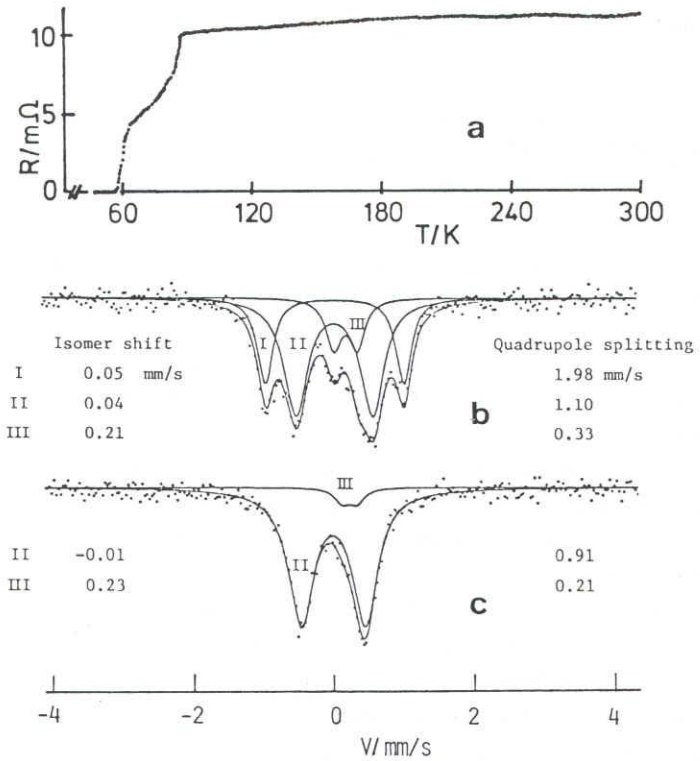

Fig.7 Temperature dependence of the resistance of $YBa_2Cu_{2.7}Fe_{0.3}O_z$ annealed at 900°C and PO_2=50Kbar (a) and the Mossbauer spectra of the same composition annealed at 300°C and PO_2=100bar (b) and at 900°C and PO_2=50kbar. The Mossbauer spectra were obtained at room temperature.

high temperature as seen in Fig.7(a) after annealing at PO_2=50kbar, though the sample annealed only at 100bar remained semiconductive at least down to 30K. The ac susceptibility confirmed in its field and temperature dependence that small superconducting regions appeared below 87K which were coupled just below 60K, thus corresponding to the resistance drop in two steps. The lattice constants changed to c=3a after the annealing. In addition, there appeared several weak peaks between the main peaks, which we have supposed to be satellite peaks corresponding to some kind of ordered domain structure.

It is interesting to note that the T_c seems to be saturated at about 90K over a wide Fe content range. Because microdomain structure is expected to be formed to stabilize impurity atoms in the boundaries and because both Fe and Co prefer octahedral coordination to such a square planer coordination in which Cu(1) and Cu(2) are stabilized, we suppose that these impurity atoms and excess oxygen cooperatively tend to be located in the domain boundaries on annealing at high oxygen pressures. In fact, Mossbauer spectrum of $YBa_2Cu_{2.7}Fe_{0.3}O_z$ drastically changed to an almost single component after annealing at PO_2=50kbar at 900°C, high enough to facilitate atomic diffusion, indicating that almost all the Fe ions are stabilized in unique sites (Fig.7(b) and (c))(a similar change was reported for samples with $x \leq 0.12$ annealed at PO_2=100bar[14]). The T_c, then, can recover its original value because the interior of domains are cleaned up. The short superconducting coherence length allows it.

5.$YBaSrCu_3O_{7+z}$[17]

Oxide belonging to the $YBa_2Cu_3O_z$ family easily intercalate and deintercalate oxygen atoms into and from their latticcs as shown above. However, $YBa_2Cu_3O_{6.9}$ once prepared in an oxygen stream of 1 atm at 400 – 500°C hardly absorbs oxygen even at PO_2 = 600bar[18]. On the other hand, we have found that $YBaSrCu_3O_z$, where a half of the barium of $YBa_2Cu_3O_z$ is replaced by strontium, shows a more enhanced oxygen insertion under similar conditions. As reported by many research groups, $YBaSrCu_3O_z$ behaves similarly to $YBa_2Cu_3O_y$ under normal oxygen pressure[19,20]; the high temperature – low oxygen content phase shows tetragonal symmetry and is semiconductive, while the low temperature – high oxygen content phase is orthorhombic and superconducting (Tc = 80K). Under high oxygen pressure, oxygen content exceeds 7.0 and, at the same time, structure as examined by X-ray diffraction(XRD) becomes tetragonal again.

Table I Annealing condition, oxygen content, and structure of $YBaSrCu_3O_z$

annealing temperature (C)	oxygen pressure (bar)	time (h)	composition (z)**	structure* (XRD)
950	0.2	6	6.20	T
900	1	12	6.32	T
800	1	24	6.41	T
700	1	24	6.54	T
600	1	40	6.71	O
500	1	48	6.79	O
400	1	60	6.90	O
400	1	100	6.95 ***	O
400	500	60	6.97	O
350	500	60	7.00	T
300	100	72	7.10	T
300	500	155	7.17	T
300	600	144	7.20	T
900	50000	0.5	7.30	T

* T : tetragonal O : orthorhombic
** standard deviation of the coulometric titration is 0.03-0.04
*** slow cooling in a furnace

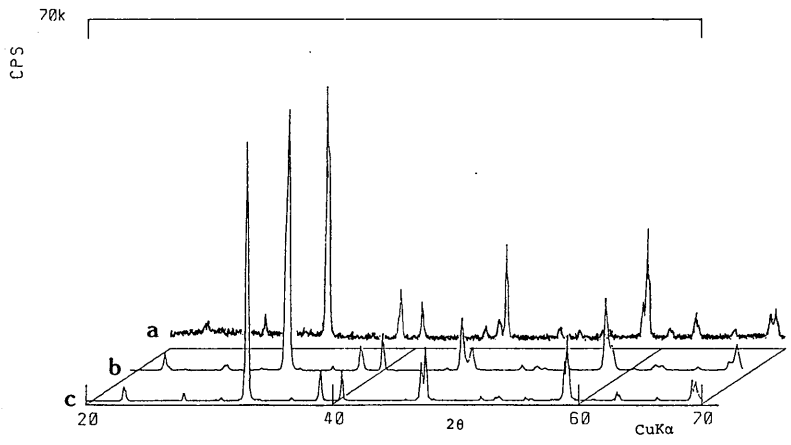

Fig 8. X-ray diffraction patterns of (a)$YBaSrCu_3O_{6.20}$(T), (b)$YBaSrCu_3O_{6.90}$(O), and (c) $YBaSrCu_3O_{7.20}$(T)

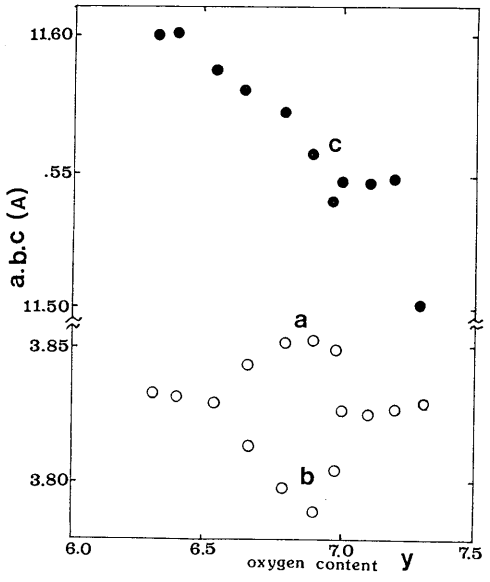

Fig 9. Variation of the lattice parameters with oxygen content for $YBaSrCu_3O_z$.

Data listed in Table 1 indicate how the oxygen content varies with the equilibrating conditions. XRD measurements (see Fig.8), indicated three kinds of phases depending on oxygen content; a tetragonal phase with low oxygen contents, $z<6.6$, an orthorhombic phase for $6.6<z<7.0$, and a new tetragonal phase with highest oxygen contents, $z>7.0$. The two tetragonal phases on either side of the orthorhombic phase strongly resemble each other except the point that the a and c-axes are both shorter in the oxygen rich side.

Figure 9 shows the remarkable dependence of the lattice parameters upon oxygen content. The tetragonal to orthorhombic transition with increasing z occurs at $z=6.6$, as also reported by Ono et al[20]. The orthorhombic distortion increases with increasing oxygen content reaching the maximum at $YBaSrCu_3O_{6.9}$ formed at 400°C under 1bar of oxygen. However, further oxygen insertion under high oxygen pressure leads to a decrease in orthorhombicity as clearly noticed from decreasing separations between the following pairs

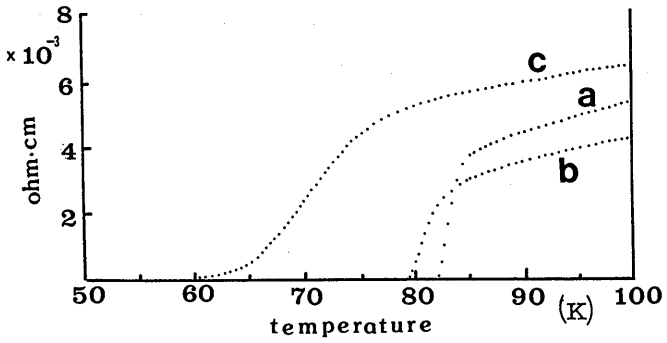

Fig 10. Temperature dependence of resistivity for $YBaSrCu_3O_z$; a) z = 6.90, b) z = 7.20, and c) z = 7.30

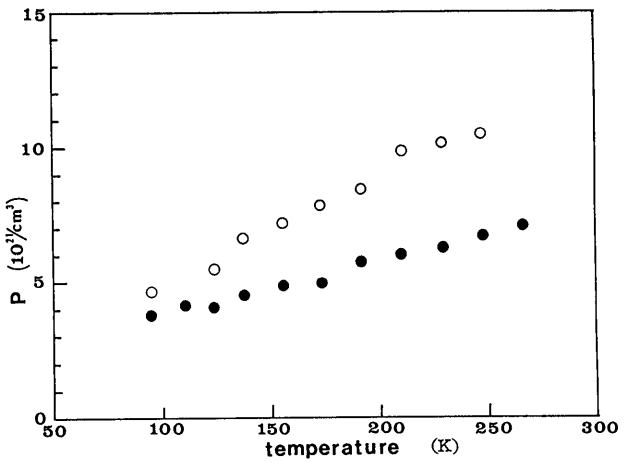

Fig 11. Temperature dependence of the effective hole concentration $P_H(= 1/R_He)$ for z = 6.90(○) and z = 7.20(●).

of the XRD peaks; (i) 103 and 013+110, (ii) 006+200 and 020, and (iii) 116+213 and 123. For z>7.0 attained at 350°C and PO_2 = 100bar, the lattice symmetry becomes tetragonal within experimental error. Such an oxygen rich tetragonal phase has been found when trivalent lanthanide ions partially substitute for divalent barium as in $La_{1+x}Ba_{2-x}Cu_3O_z$[21], $Nd_{1+x}Ba_{2-x}Cu_3O_z$[22], and $YBa_{2-x}La_xCu_3O_z(x>0)$[23]. In these cases, excess oxygen is introduced in Cu(1)–O layers to compensate the excess positive charge due to the substitution. In these phases the apparent oxidation state of copper remains almost unchanged, while in $YBaSrCu_3O_z$ (z>7.0), it may be expected to increase with the increase in z.

The superconducting transition studied by resistivity measurements is illustrated as a function of oxygen content in Fig.10. The transition temperature is considerably decreased and the transition width becomes broad as y increases. Figure 11 shows the temperature dependence of the effective hole concentration $P_H(= 1/R_H)$ for z = 6.90 and 7.20. Both samples show a strong temperature dependence which is common to the 90K class $LnBa_2Cu_3O_z$ family. The R_H decreased to $3.9x10^{21}/cm^3$ at z = 7.2 from $4.9x10^{21}/cm^3$ at z = 6.90 (at 100K), the decrease being compatible with the Tc change.

Microscopic structure of "tetragonal" $YBaSrCu_3O_{7.20}$ was studied in detail by TEM from the view point same as the case of $YBa_2Cu_{3-x}Fe_xO_z$. Shown in Fig.12 are the TEM images and diffraction spots for z = 6.90 and 7.20. The diffraction spots for y = 6.90 are clearly split and a well-known type of twin structure

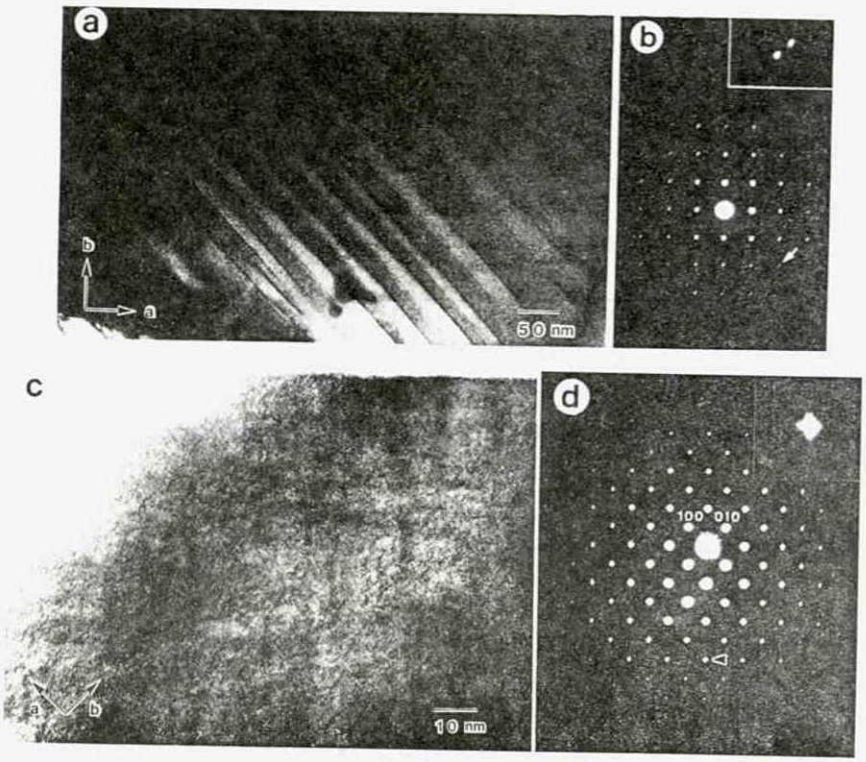

Fig 12. Electron micrographs and electron diffraction patterns with the [001] beam axis for z = 6.90(a,b) and z = 7.20(c,d)

consisting of orthorhombic bands appear homogeneously in the TEM image. On the other hand, no spot-splittings were found for z = 7.20, but the spots are streaked along the $[110]^*$ and $[1\bar{1}0]^*$ direction, just as observed for $YBa_2Cu_{3-x}Fe_xO_z$ with x>0.03, suggesting local ordering of 1-D Cu(1)-O chains along the [100] or [010] direction. However, the corresponding TEM image shown in Fig.12(c) does not show such a well-defined cross-hatched or "tweed" pattern as observed for the Fe-doped $YBa_2Cu_3O_z$. Good coherence of the domain boundaries in multiple Cu(1)-O planes stacked along the c-axis is required for such a cross-hatched pattern. Probably the coherence is lacking in the present sample. It is interesting to note here that a well-defined tweed pattern was observed in a sample annealed insufficiently, i.e. for a shorter time, from which a microdomain size in the ab plane of 10^5A^2 was estimated. With increasing annealing time and, therefore, increasing oxygen content, microdomains seem to become much smaller and, at the same time, the coherence along the c-axis of the boundaries seem to become poor. "Tetragonal" symmetry detected by XRD is again nothing but an averaged one.

Microdomain structure is expected to be formed to accommodate excess oxygen in the domain boundary region without altering the inside. The copper ions in the boundary region would be coordinated octahedrally (Fig.6(c)). A simple calculation shows that oxygen content can be raised in this way up to z = 7.20 for $50x50A^2$- sized microdomains. However, such a local coordination allowing the presence of oxygen atoms in the nearest neighboring sites has been suggested by Manthiram et al.[23] to reduce the hole concentration by trapping them in peroxide ions, $(O_2)^{2-}$. We agree with this, considering the Hall effect results shown in Fig.11. However, Tc was not seriously reduced, because the domain size remained large enough in comparison with the short coherence length of order of 10A. Degradation of the intergrain coupling as revealed in the broadened transition width[14,24] has been interpreted as resulting from the degradation of the intragrain superconducting properties due to the change in microstructure and the decrease in the hole concentration.

5. $La_{2-x}A_xCuO_{4+z}$[25,26]

Oxygen stoichiometric La_2CuO_4 is an antiferromagnet with a T_N around 250–300K[27,28], while superconductivity has been observed for oxygen-doped $La_2CuO_{4+z}(z>0)$ at around Tc = 40K[29–31]. The Tc is almost the same as observed for alkaline earth-substituted $La_{2-x}A_xCuO_4$ (A=Ba,Sr,Ca). The superconducting volume fraction of La_2CuO_{4+z} is increased by annealing under oxidizing conditions. Jorgensen et al. proposed a phase diagram of La_2CuO_{4+z} from their powder neutron diffraction work[32,33]. According to them, a phase separation into nearly stoichiometric Bmab (z=0) and oxygen rich Fmmm phases occurs for $0<z<0.08$ at relatively low temperature. Mixed-phase samples in this range display both antiferromagnetic and superconducting behaviors (see Fig.13).

Such an oxygen excess in K_2NiF_4 structure has been known for La_2NiO_{4+z} and La_2CoO_{4+z}, too[34]. Two types of ordering modes leading to serial oxygen contents have been found for La_2NiO_{4+n} (n=1/2n: n>2)[35], while any such ordering has not been reported for La_2CuO_{4+z}.

The excess-oxygen defect in La_2MO_{4+z} (M = Co, Ni, Cu) may be caused by the bond-length mismatch between the LaO and MO_2 layers. A measure of the bond-length matching is the tolerance factor,

$$t = (La - O)/\sqrt{2}(M - O)$$

where the La–O and M–O bond lengths are commonly taken as the sums of the empirically determined ionic radii. The perfect epitaxial matching of the bonds occurs for t=1. However, the values for $La^{3+}+O^{2-}$ and $\sqrt{2}(Cu^{2+}+O^{2-})$, for example, are 2.58 and 2.86A, respectively, according to Shannon and Prewitt[36]. Generally, $t \cong 0.9$. The CuO_2 planes are thus under compression and the LaO planes under tension. The internal stress within a CuO_2 plane may be relieved by a cooperative tilting of the CuO_6 octahedra making the Cu–Cu distance shorter, when the crystal structure is distorted from tetragonal to orthorhombic symmetry, while introduction of excess oxygen between a pair of LaO planes expands the $(LaO)_2$ lattice and eases the tension[37]. Moreover, the excess oxygen, if it exists as oxide ions, not as peroxide ions, oxidizes and, thereby, contracts the CuO_2 sheet, thus relaxing the bond-length mismatch[37].

In this study, we prepared a few solid solution systems, $La_{2-x}A_xCuO_4$ where A = Nd and Bi, and tried to dope the excess oxygen in the structure. The reasons why we substituted the metals, Nd and Bi are as follows. (A) If La^{3+} ions are partially replaced by smaller rare-earth ions like Nd^{3+}, the bond-length mismatch will be further enhanced. It may then be expected that excess oxygen is more easily introduced

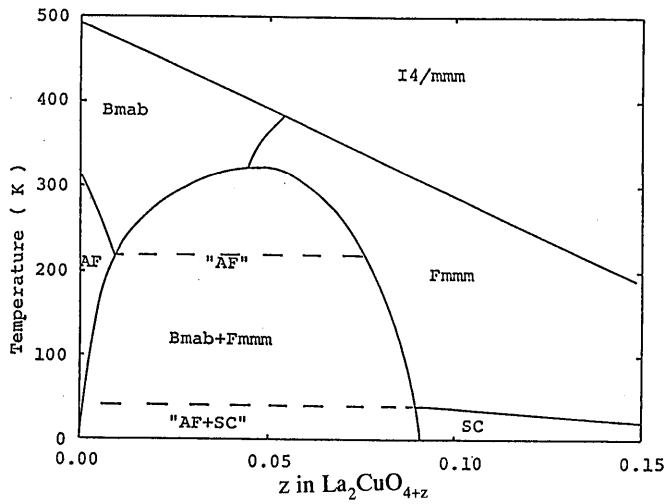

Fig.13 The miscibility gap for La_2CuO_{4+z}. From ref(33).

within the double rock salt layer. (B) Bi^{3+} has a similar size but a different electrical configuration in comparison with La^{3+}. Bi^{3+} ion has the "inert 6s electrons" due to the "inert pair effect" proper to heavy p-block metals. The character is largely different from lanthanide 3+ ions. $La_{2-x}Bi_xCuO_4$ has been prepared by

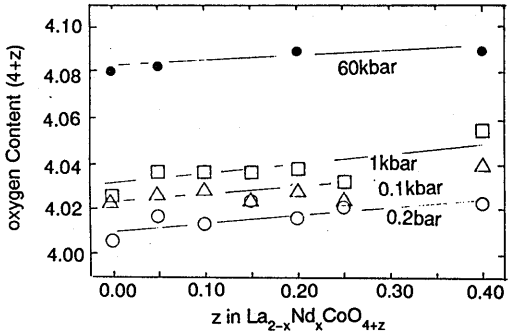

Fig.14. Variation of oxygen content with oxygen pressure in $La_{2-x}Nd_xCuO_{4+z}$.

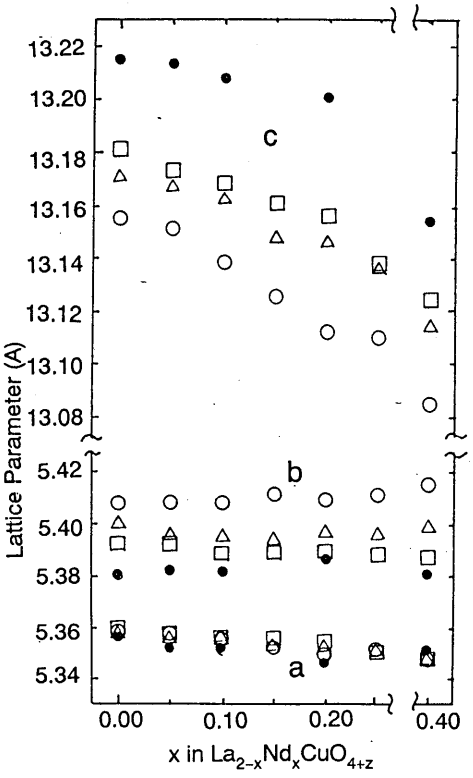

Fig.15. Lattice parameters for $La_{2-x}Nd_xCuO_{4+z}$ prepared under various oxygen pressures. ○,0.2bar,△,0.1kbar,□,1kbar, ●,60kbar.

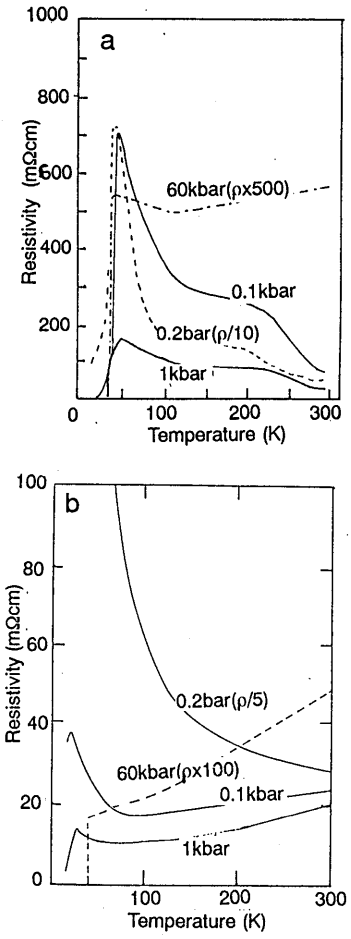

Fig.16. Variation of electrical resistivity on the oxygen pressure for $La_{2-x}Nd_xCuO_{4+z}$. a) x=0, b) x=0.2 (right)

some authors[38,39], but no superconducting behavior has not been reported. We found the superconductivity, however, by treating the samples under the oxygen pressure of only few hundred bar.

Two kinds of methods were carried out in order to dope the oxygen in the K_2NiF_4 structure; the annealing under high oxygen pressure at high temperature and the electrochmical oxidation in an aqueous alkaline solution at ambient temperature. For the latter method, it has been known that the oxygen is easily intercalated into the oxygen-deficient perovskite[40]. Recently, Grenier et al. applied this method to La_2CuO_4[41]. In this study, we prepared the excess oxygen doped $La_{2-x}A_xCuO_{4+z}$ (A=Nd and Bi) having various oxygen content by the annealing under high oxygen pressure and electrochemical oxidation, comparing their crystal structures and electrical behaviors.

(A) High oxygen pressure effect —— $La_{2-x}A_xCuO_{4+z}$ (A=Nd,Bi)

As shown in Fig.14, the oxygen content increases with increasing oxygen pressure and reaches 4.08–4.09 under 60kbar of oxygen pressure. Under a given oxygen pressure, it increases with increasing Nd content as expected, but the degree is not so large as to change the doped hole content drastically. The variation of the orthorhombic lattice parameters with Nd content, x, at room temperature are plotted in Fig.15. The orthorhombic La_2CuO_4 structure was found for $0 \leq x \leq 0.4$, while a T'-Nd_2CuO_4 phase coexisted for $x>0.40$. Within the monophasic region, the c parameter considerably decreases as a size effect of the Nd ions, while the a and b parameters show, respectively, a slight decrease and increase. On the other hand, the introduction of excess oxygen makes the c parameter increase and the b parameter decrease. The oxidation may thus be said to counteract the Nd–substitution from the viewpoint of structure chemistry as expected. However, the XRD data measured at 300K show no evidence of such a transformation from Bmab to Fmmm with increasing oxygen content as proposed for La_2CuO_{4+z} by Jorgensen et al. Neither was any separation into nearly stoichiometric $La_{2-x}Nd_xCuO_4$ and oxygen-rich $La_{2-x}Nd_xCuO_{4+z}$ observed at room temperature.

Figure 16 shows the electrical resistivity data for $La_{2-x}Nd_xCuO_{4+z}$ with x = 0, and 0.2 prepared under various oxygen pressures. Typical features revealed here are as follows. i) All the La_2CuO_{4+z} samples after the present oxygen pressure treatments are, at least partially, superconducting. The onset transition temperature where resistivity begins to drop is almost invariant whatever the oxygen pressure is, though the normal-state resistivity decreases and becomes more metallic with increasing oxygen content. The resistance anomaly in the 150–300K range, which has been attributed to the phase separation involving oxygen diffusion[42], gradually disappears. ii) In the Nd-substituted samples, the normal state resistivity tends to decrease with increasing Nd content under the same preparative conditions (that is, at almost the same oxygen content). For example, even after the treatment under 1kbar of oxygen, non-substituted $La_2CuO_{4.025}$ shows semiconductive behavior with a broad resistive anomaly in the 150–300K range, while at x=0.2, the normal state resistivity is almost metallic. iii) In spite of the more metallic behavior in the normal state, Tc decreases as the Nd content increases. $La_2CuO_{4.005}$ prepared in air shows a sign of superconductivity at around 40K, but $La_{1.8}Nd_{0.2}CuO_{4.01}$ shows no superconductivity down to 10K.

In Fig.17, the variation of Tc with excess oxygen content z is shown. The Tc of La_2CuO_{4+z} is independent on z, while that of $La_{2-x}Nd_xCuO_{4+z}$ depends strongly on z.

Figure 18 shows the temperature dependence of magnetic susceptibility (magnetization divided by applied field) measured on cooling. For samples of low excess oxygen contents it is difficult to find a well-defined, sharp transition because the superconducting volume fraction is small. The substitution of Nd for La and the use of higher oxygen pressures increase the volume fraction of the superconducting phase. For $La_2CuO_{4.08}$ and $La_{1.8}Nd_{0.2}CuO_{4.09}$ prepared under 60kbar of oxygen, the susceptibility is -4.9×10^{-4}emu/g and -1.8×10^{-3}emu/g at 4K, respectively.

Since the oxygen content prepared under the same oxygen pressure shows no large dependence upon x, i.e. the doped hole content is considered to be nominally almost the same, it is surprising and interesting that the superconducting volume fraction is largely increased by the Nd-substitution. The relatively low resistivity for the Nd-doped samples in their normal state can also be explained by the increase of

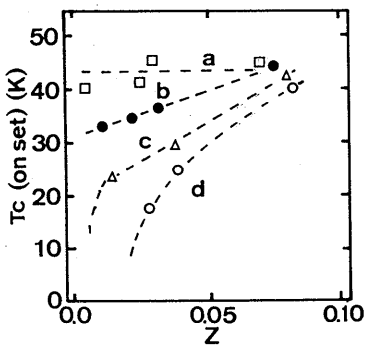

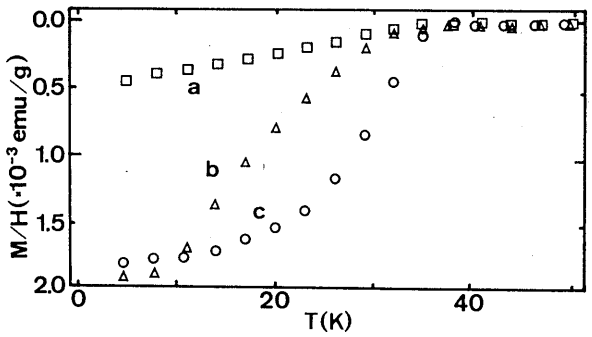

Fig.17. Variation of the on-set Tc with excess oxygen content for $La_{2-x}Nd_xCuO_{4+z}$. (left)

Fig.18. Magnetic susceptibility of $La_{2-x}Nd_xCuO_{4+z}$ measured on cooling in a field of 10G. (right)

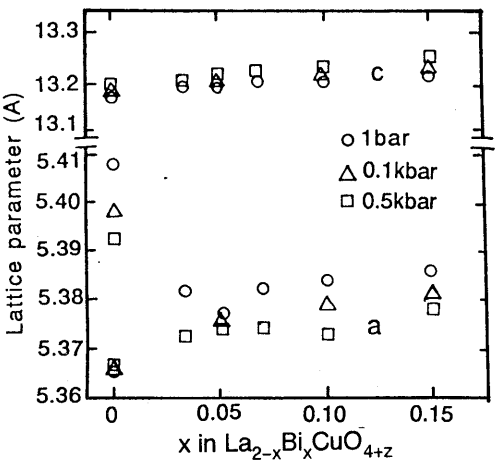

Fig.19. Lattice parameters for $La_{2-x}Bi_xCuO_{4+z}$

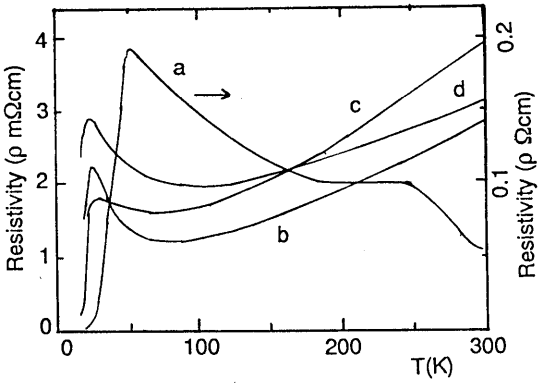

Fig.20. Electrical resistivity for $La_{2-x}Bi_xCuO_{4+z}$
a) x=0, b)x=0.05, c)x=0.10, d)x=0.15

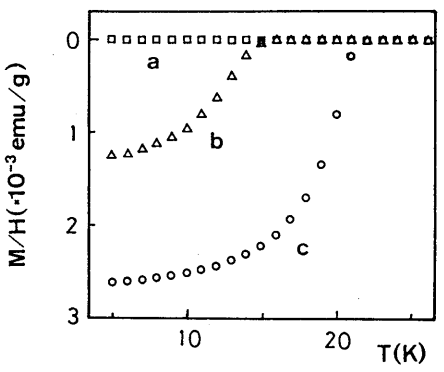

Fig.21. Magnetic susceptibility of $La_{1.95}Bi_{0.05}CuO_{4+z}$ measured on cooling in a field of 10G..
a)z=0.01(1bar), b)z=0.03(0.1kbar), c)z=0.06(0.5kbar)

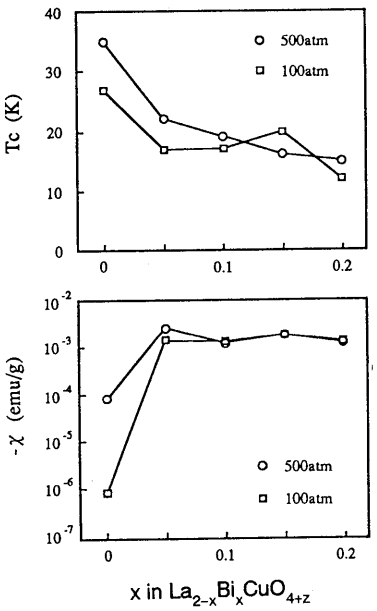

Fig.22. Bi content dependencies of Tc and magnetic susceptibility at 5K.(right)

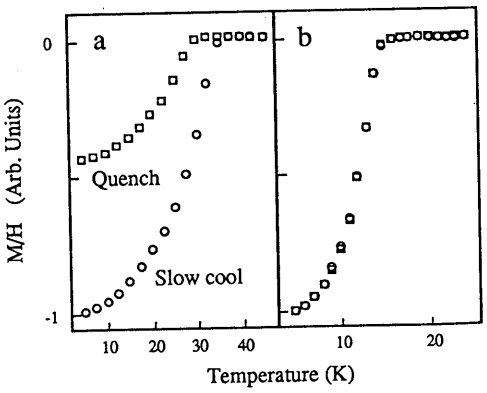

Fig.23. Cooling rate dependence of the Meissner curve for x=0(a) and x=0.05(b) treated at PO_2=0.5kbar.

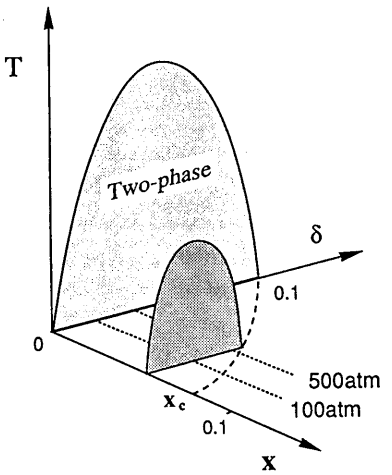

Fig.24. Schematic representation of a probable phase diagram for $La_{2-x}Bi_xCuO_{4+z}$. The miscibility gap existing in x=0 tends to close with increasing x.

the fraction of the superconductive phase.

Such a large fraction can be attained much more easily, i.e. at a much lower oxygen pressure of 500atm for $La_{2-x}Bi_xCuO_{4+z}$. The solid solution range was less than x=0.2, unknown extra peaks appeared for x=0.25. In Fig.19, the variation of lattice parameters with Bi content, x, are plotted. The orthorhombic La_2CuO_4 structure rapidly changes to tetragonal K_2NiF_4 form with the substitution of Bi. Within the mono-phasic region, the both a and c parameters slightly increases, probably due to the larger ionic size of Bi^{3+} than La^{3+}. With the treatment of oxygen pressure, a axis decreases while c axis increases slightly.

The solid solution $La_{2-x}Bi_xCuO_{4+z}$ showed superconductivity only after being annealed under high oxygen pressures, implying an excess oxygen dopes the CuO_2 plane with carrier holes. Figure 20 shows the electrical resistivity data with x=0, 0.05 0.10 and 0.15 prepared under 0.5kbar of oxygen pressure. The broad hump around 200-250K which has been attributed to the phase separation is absent for x>0.05.

Figure 21 displays the temperature dependence of magnetic susceptibility for x=0.05. As the annealing oxygen pressure increases, both the onset temperature Tc and the diamagnetic response increase. The value of $\chi_g = -2.618x\ 10^{-3}$ emu/g for PO_2=0.5kbar corresponds to a superconducting volume fraction of 12%, which is comparable with those of the $La_{2-x}A_xCuO_4$ (A=Ba, Sr) system. Such a large fraction can be attained for $La_{2-x}Nd_xCuO_{4+z}$ but needs much higher oxygen pressure of 60kbar[25]. Figure 22 shows x dependence of Tc and the volume fraction. As x increases from 0 to 0.2, Tc decreases at first and then slowly decreases. As for the effects of different annealing oxygen pressures, Tc always changes by 3-5K, while the difference in the volume fraction is large only for x<0.05. The phase separation in La_2CuO_{4+z} is reflected in its M/T vs T curve as a cooling rate dependence as shown in Fig.23. A powdered sample was at first cooled from room temperature to 5K in about 10s, warmed up to 60K, and then magnetization was measured in a field of 10G on cooling("quench"). After that, the sample was warmed to 350K, slowly cooled to 60K with an average cooling rate of 0.5K/min and magnetically measured on cooling("slow cool"). In the case of La_2CuO_{4+z}, a significant change of the superconducting properties was observed. Tc raised by 3K and the diamagnetic signal was about twice after the slow cooling. On the other hand, such a change was not detected in the Bi doped samples.

All these data for $La_{2-x}A_xCuO_{4+z}$ with A=Nd and Bi suggest consistently that the phase separation for La_2CuO_{4+z} is suppressed by a random potential in the rock salt layer, allowing the formation of a superconducting phase that changes its Tc depending upon the carrier concentration. Figure 24 shows a tentative x-z-T phase diagram. The miscibility gap existing between z≃0 and 0.1 for x=0 diminishes as x

increases and disappears at a critical substitution content x_c:x_c may be between 0.05 and 0.10. For $0<x<x_c$ two phases exist at low temperatures:antiferomagnetic $La_{2-x}A_xCuO_{4+z}$ and superconducting $La_{2-x}A_xCuO_{4+z'}$. z' in the latter decreases but the Meissner signal increases with x in the two phase region. The slight decrease in Tc for x>0.05 may partly be due to the randomness caused by the substitution.

(B) Electrochemical oxidation —— La_2CuO_{4+z} and $La_{2-x}Bi_xCuO_{4+z}$

The electrical oxidation was carried out in a 1N KOH aqueous solution at room temperature. The cell consists of three electrodes; the working electrode was a La_2CuO_4 sintered disk (2mm thick and 8mmΦ) annealed under 0.1kbar of oxygen at 600°C for 80hr in advance, which was connected to the lead with Ag paste covered by the epoxy-resin, Ag/AgCl electrode (E°=0.2223V vs. NHE) was used as a reference electrode and the counter electrode was a platinum sheet (10mmx10mmx0.5mm). The electrolysis was carried out at 25°C in air for 24-48hr.

XRD powder patterns for the typical samples of La_2CuO_{4+z} annealed under high oxygen pressure and oxidized electrochemically are compared in Fig.25. The XRD patterns of the surface of the electrochemically oxidized pellets show no significant difference with those of the crashed powdered samples, indicating that the electrochemical reaction occurs homogeneously in the sintered pellet. The variation of the splitting of (200) and (020) or (204) and (024) reflections shows that the oxygen pressure treatment brings the decreased orthorhombic distortion, while the electrochemical oxidation under high electrode potential exhibits the more enhanced orthorhombic distortion. In Fig.26 is shown the variation of lattice constants on the treated oxygen pressure(Fig.26(a)) and the electrode potential applied(Fig.26(b)). The oxidized samples by both methods have the increased c-axis compared to that of stoichiometric La_2CuO_4. As shown in Fig.27, the value of c-axis can be seen as the exact measure of the excess oxygen content of La_2CuO_{4+z}. The c-parameter increases linearly with the increasing oxygen content even if the oxidized processes are different. The variation of a and b parameters on the oxygen content, however, shows the different behaviors between high pressure oxygenated and electrochemically oxygenated La_2CuO_{4+z}.

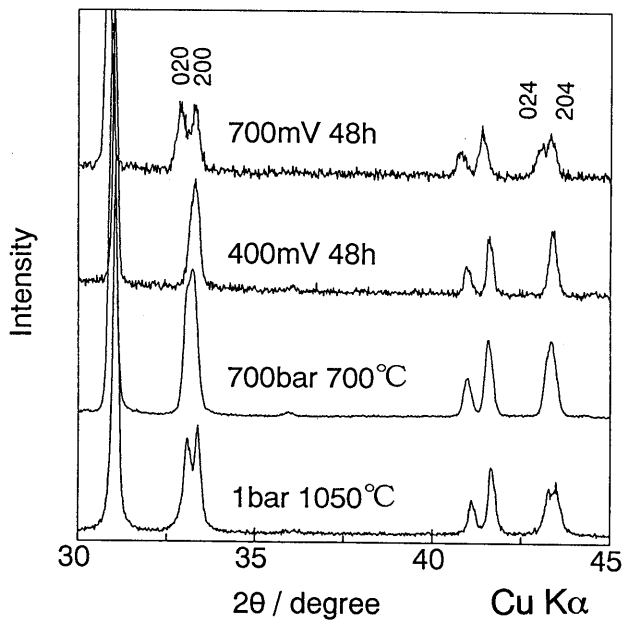

Fig.25. XRD patterns for La_2CuO_{4+z} prepared by high oxygen treatment and electrochemical oxidation.

Figure 28 shows the electrical resistivity data for La_2CuO_{4+z} prepared by the electrochemical method. The dependence on the oxygen content is almost similar to those prepared under high oxygen pressure(Fig. 16(a)), however, the magnetic susceptibility for the electrochemical oxidation shows larger fraction as shown in Fig.29. The difference in the orthorhombicity and volume fraction seen in the samples having same oxygen content but prepared by different route may be due to the difference in the nature of doped oxygen, that is, oxide ions or peroxide ions and the distribution in La_2CuO_4 structure.

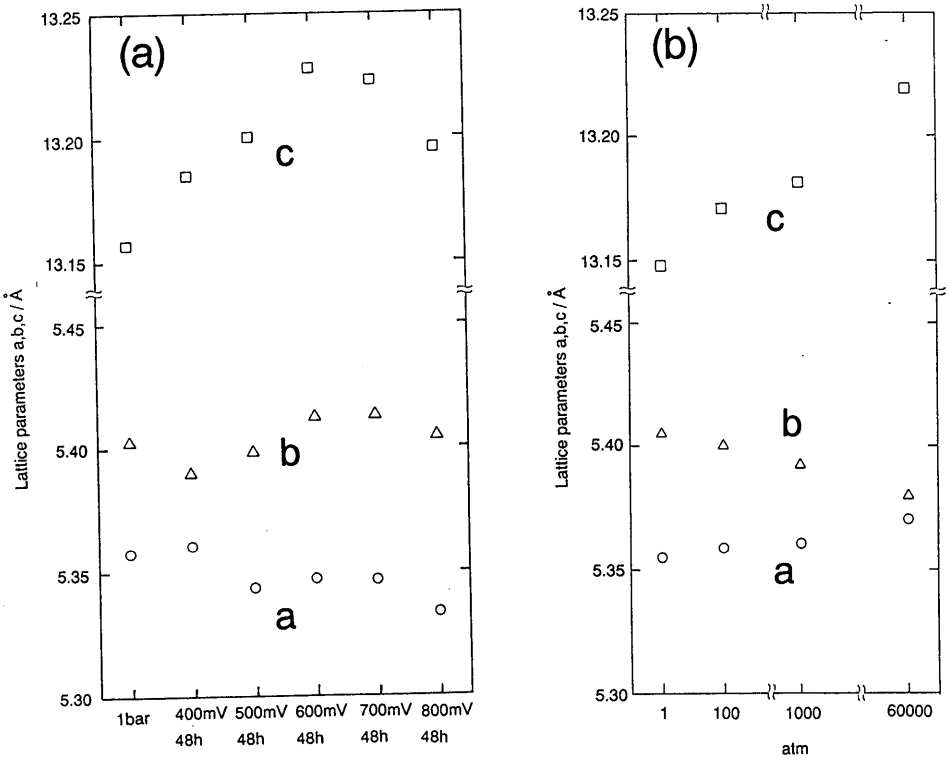

Fig.26. Variation of lattice constants for La_2CuO_{4+z} on the electrode potential(a) and the treated oxygen pressure(b).

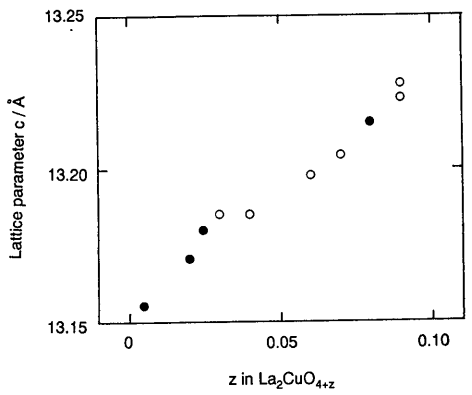

Fig.27. Variation of c-parameter for La_2CuO_{4+z} with excess oxygen content. ●:High oxygen pressure treatment, O:Electrochemical oxidation

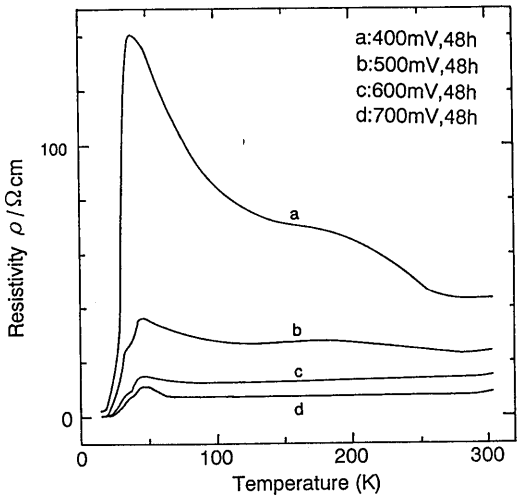

Fig.28. Electrical resistivity for La_2CuO_{4+z} after electrochemical oxidation.

The electrochemical oxidation is also effective to bring the superconductivity in $La_{2-x}Bi_xCuO_{4+z}$. Figure 30 shows the magnetic susceptibility of the sintered samples for $La_{1.93}Bi_{0.07}CuO_{4+z}$ treated at the various electrode potentials. Some samples show the Tc on set of 30K, while that of annealed under 500atm of oxygen is less than 20K. Only a few hundred mV of electrode potential has a more oxidation power than considerable high oxygen pressure. The electrochemical reaction can be said to be the simple and easy way to realize the oxygen doped state in the perovskite type superconductors.

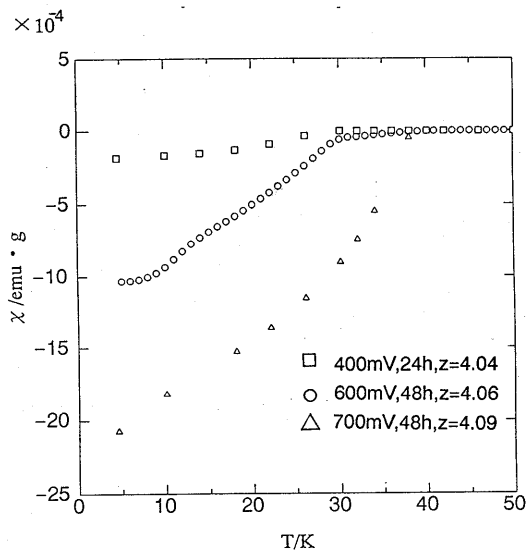

Fig.29. Magnetic susceptibility of La_2CuO_{4+z} after electrochemical oxidation.

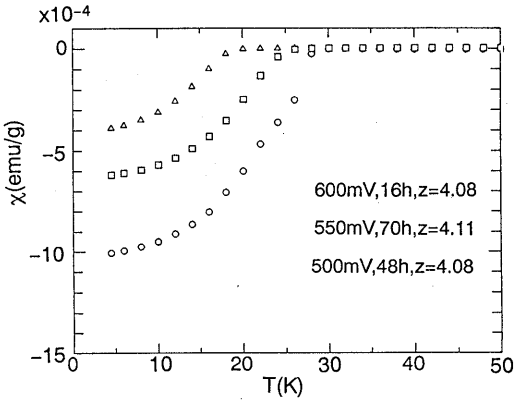

Fig.30. Magnetic susceptibility of $La_{1.93x}Bi_{0.07}CuO_{4+z}$ after electrochemical oxidation.

Acknowledgements

The original works were made by the collaboration with colleges of Kyoto University who are Profs. M. Takano and Y. Bando and Dr. Z.Hiroi. The authors also thank Mr. A.Sato, Y.Mukai, H. Hashimoto, H.Tomida and K.Yoshikawa in Yamamoto Laboratory for their contribution to this work. This study was financially supported by " Grant-in-Aid for Scientific Research on Chemistry of New superconductors" from the Ministry of Education, Science, and Culture.

Reference

[1] J.G.Bednorz and K.A.Muller, Z. Phys. B-Condensed Matter, 64, (1986) 189.
[2] M.Takano, M.Azuma, Z.Hiroi, Y.Bando and Y.Takeda, Physica C, 176, (1991) 441.
[3] S.Kume, F.Kanamaru, Y.Shibasaki, M.Koizumi, K.Yasunami and T.Fukuda, Rev. Sci. Instruments, 42 (1971) 1856.
[4] Y.Takeda, S.Naka, M.Takano, S.Shinjo, T.Takada and M.Shimada. Mat. Res. Bull., 13 (1978) 61.
[5] Y.Takeda, H.Hasimoto, A.Sato, N.Imanishi and O.Yamamoto, J. Jpn. Soc. Powder & Powder Metallurgy, 39, (19929 345.
[6] G.Demazeau, C.Parent, M.Pouchard and P.Hagenmuller, Mat. Res. Bull., 7, (1972) 913.
[7] J.B.Goodenough, N.F.Mott, M.Pouchard, G.Demazeau and P.Hagenmuller, Mat. Res. Bull., 8, (1973) 647.

[8] J.F.Bringley, B.A.Scott, S.J.La Placa, R.F.Boehme, T.M.Shaw, M.W.McElfresh, S.S.Trail and D.E.Cox, Nature, 347, (1990) 263.

[9] M.Arjomand and D.J.Machin, J. Chem. Soc. Dalton, (19759 1061.

[10] R.J.Cava, T.Siegrist, B.Hessen, J.J.Krajewski, W.F.Peck.Jr. B.Batlogg, H.Takagi, J.V.Waszczak, L.F.Schneemeyer and H.W.Zandbergen, J. Solid State chem., 94, (1991) 170.

[11] M.Takano, Z.Hiroi, H.Mazaki, Y.Bamdo, Y.Takeda, R.Kanno, O.Yamamoto, Y.shimakawa and M.Shimada, Proc. MRS Int. Meet. Adv. Mat., 6, (1989) 433.

[12] Y.Maeno, T.Tomita, M.Kyogoku, s.Awaji, y.Aoki, K.Hoshino, A.Minami and T.Fujita, Nature, 328 (19879 512.

[13] Y.Shimakawa, Y.Kubo, K.Utsumi, Y.Takeda and M.Takano, Jpn. J. Appl. Phys., 27 (1988) L1071

[14] Z.Hiroi, M.Takano, Y.Takeda, R.Kanno and Y.Bando. Jpn. J. Appl. Phys., 27 (1987) L403.

[15] M.Takano, H.Mazaki, Z.Hiroi, Y.Bando, Y.Takeda and O.Yamamoto, J. Cer. Soc. Jpn., 96, (1988).

[16] N.Nakayama, M.Takano, S.Inamura, N.Nakanishi and K.Kosuge, J. Solid State Chem., 11, (19879 403.

[17] Z.Hiroi M.Takano, Y.Takeda, R.Kanno and Y.Yamamoto, Jpn. J. Appl. Phys., 28, (1988) L580.

[18] Y.Takeda, R.Kanno, O.Yamamoto, M.Takano, Y.Ikeda and Y.Bando, J. Jpn. Soc. Powder and Powder Metallurgy.,34, (1987) 60.

[19] T.Wada, S.Adachi, O.Inoue, S.Kawashima and T.Mihara. Jap. J. Appl. Phys. 26 (1987) L1475.

[20] A.Ono, T.Tanaka, H.Nozaki and Y.Ishizawa, Jpn. J. Appl. Phys., 26 (1987) L1687.

[21] E.Takayama-Muronachi, Y.Uchida, A.Fujimori and K.Kato, Jpn. J. Appl. Phys., 26 (1987) L1546.

[22] S.Takekawa, H.Ozaki, Y.Ishizawa and N.Iyi, Jpn. J. Appl. Phys., 26, (1987) L2067.

[23] A.Manthiram, X.X.Tang and J.B.Goodenough, Phys. Rev.B, 37, (1988) 3734.

[24] H.Mazaki, M.Takano, Y.Ikeda, Y.Bando, R.Kanno, Y.Takeda, and O.Yamamoto, Jpn. J. Appl. Phys., 26 (1987) L1749.

[25] Y.Takeda, K.Yoshikawa, O.Yamamoto and M.Takano, J. solid State Chem., 92 (1991) 241.

[26] Y.Takeda, A.Sato, K.Yoshikawa, N.Imanishi, O.Yamamoto, M.Takano, Z.Hiroi and Y.Bando, Physica C, 185/189, (1991) 603.

[27] D.C.Johnston, J.P.Stakes, D.P.Goshrn, and J.T.Lewandowski, Phys.Rev., **B36**, (1987) 4007.

[28] R.L.Greene, H.Maletta, T.S.Plaskett, J.G.Bednorz and K.A.Muller, Solid State Commun., **3**, (1987) 379.

[29] J.E.Schirber, B.Morison, R.M.Merrill, D.E.Hlava, E.L.Venturini, J.F.Kwak, D.J.Nigrey, B.J.Baugham and D.S.Gingley, Phys. C, **158** (1989) 183.

[30] C.Chaillout, S-W.Cheng, Z.Fisk, M.S.Lehman, M.Marezio, B.Morosin, and J.E.Schirber, Phys. C, **158** (1988) 824.

[31] G.Demazeau, F.Tresse, Th.Plante, B.Chevalier, J.Etourneau, C.Michel, H.Hervieu, B.Raveau, P.Lejay, A.Sulpice, and R.Tuornier, Phys. C, **153- 155** (1988) 824.

[32] J.D.Jorgensen, B.Dabrowski, Shiyou Pei, D.G.Hinks, L.Sederholm, B.Morosin, J.E.Schirber, E.L.Venturi ni, and D.S.Ginley, Phys. Rev. **B38** (1988) 11377.

[33] B.Dabrowski, J.D.Jorgensen, D.G.Hinks, Shiyou Pei, D.R.Richards, H.B.Vanfllet and D.L.Deker, Phys. C, **162-164** 1989) 99.

[34] J.D.Jorgensen, B.Dabrowski, Shiyou Pei, P.R.Rich ards, and D.G.Hinks, Phys. Rev., **B40** (1987) 2187.

[35] Z.Hiroi, T.Obata, M.Takano, Y.Banndo, Y.Takeda and O.Yamamoyo, Phys. Rev. **B41** (1990) 11665.

[36] R.D.Shannon and C.T.Prewitt, Acta Cryst., **B25** (1969) 925. Acta Crystallogr. Sect.**B26** (1970)

1046. Acta Crystallogr. Sect **A32** (1976) 751.
[37] J.B.Goodenough and A.Manthiram, J. Solid State Chem., **88** (1990) 115.
[38] K. Fikuda, M. Sera, and M. Sato, J. Solid State Chem., **65** (1988) 1157.
[39] Chun-ming Niu, J. Dicarlo, K. Dwight, and A. Wold, J. Solid State Chem. **78** (1989) 307.
[40] T.Kudo, H.Obayashi and M.Yoshida, J. Amer. Electrochem. Soc., **124** (1977) 321.
[41] J-C.Grenier, A.Wattiaux, N.Lagueyte, J.C.Park. E.Marquestaut, J.Etourneau and M.Pouchard, Physica C, **173** (1991) 139.
[42] M.F.Hundley, J.D.Thompson, S-W.Cheong, Z.Fisk, and J.E.Schirber, Phys. Rev., B41 1990 4062.